ACS APPLIED MATERIALS & INTERFACES

Organic Electronic Devices

The Crucial Role of Fluorine in Fully Alkylated Ladder Type Carbazole Based Non-fullerene Organic Solar Cells

Qiao He, Munazza Shahid, Xuechen Jiao, Eliot Gann, Flurin Eisner, Tingmang Wu, Zhuping Fei, Thomas D. Anthopoulos, Christopher R. McNeill, and Martin J. Heeney

ACS Appl. Mater. Interfaces, **Just Accepted Manuscript** • DOI: 10.1021/acsami.0c00981 • Publication Date (Web): 30 Jan 2020

is published by the American Chemical Society. 1155 Sixteenth Street N.W., Washington, DC 20036

The Crucial Role of Fluorine in Fully Alkylated Ladder Type Carbazole Based Non-fullerene Organic Solar Cells

Qiao He,[†] Munazza Shahid,[†,▽] Xuechen Jiao,[‡] Eliot Gann,[§] Flurin D. Eisner,[∥] Tingmang Wu,[†] Zhuping Fei,[⊥] Thomas D. Anthopoulos,[#] Christopher R. McNeill,[‡] and Martin Heeney*[,†]

[†]Department of Chemistry and Centre for Plastic Electronics, White City Campus, Imperial College London, London W12 0BZ, UK

[‡]Department of Materials Science and Engineering, Monash University, Victoria 3800, Australia

[§]Materials Measurement Science Division, National Institute of Standards and Technology, Gaithersburg, MD 20899, USA

[∥]Department of Physics and Centre for Plastic Electronics, South Kensington Campus, Imperial College London, London SW7 2AZ, UK

[⊥]Institute of Molecular Plus, Tianjin Key Laboratory of Molecular Optoelectronic Science, Tianjin University, Tianjin 300072, P. R. China

[#]King Abdullah University of Science and Technology (KAUST), KAUST Solar Centre, Thuwal 23955-6900, Saudi Arabia

[▽]Department of Chemistry, School of Science, University of Management and Technology, Lahore, 54770, Pakistan

Supporting Information Placeholder

ABSTRACT: Two fused ladder type non-fullerene acceptors, DTCCIC and DTCCIC-4F, based on an electron-donating alkylated dithienocyclopentacarbazole core flanked by electron-withdrawing non-fluorinated or fluorinated 1,1-dicyanomethylene-3-indanone (IC or IC-4F), are prepared and utilized in organic solar cells (OSCs). The two new molecules reveal planar structures and strong aggregation behavior, and fluorination is shown to red shift the optical band gap and down shift energy levels. OSCs based on DTCCIC-4F exhibit a power conversion efficiency of 12.6 %, much higher than that of DTCCIC based devices (6.2 %). Microstructural studies reveal that while both acceptors are highly crystalline, bulk heterojunction blends based on the non-fluorinated DTCCIC result in overly coarse domains, while blends based on the fluorinated DTCCIC-4F exhibit a more optimal nanoscale morphology. These results highlight the importance of end group fluorination in controlling molecular aggregation and miscibility.

KEYWORDS: *organic solar cells, non-fullerene acceptors, carbazole, fluorine effect, fully alkylated side chains*

INTRODUCTION

The performance of solution processable organic solar cells (OSCs) based on non-fullerene acceptors (NFAs) has achieved impressive progress, with their power conversion efficiencies (PCEs) reaching beyond 16 % in this year for single junction devices.[1-3] Compared to fullerene derivatives, NFAs possess several intrinsic advantages including increased flexibility of tuning chemical structures, broad absorbance across the solar spectrum, easily tunable energy levels, and relatively simple purification processes.[4-6] NFAs based on a ladder type electron-donating backbone flanked with two strong electron-withdrawing endgroups have become dominate in high efficiency OSCs.[7-13]

Among many efficient molecular modulation strategies for photovoltaic applications, the introduction of fluorine atoms into NFA materials has been widely applied to adjust their optical absorption, energy levels and carrier mobility properties.[14-21] The success of this strategy is associated with several factors. First, the small size of fluorine coupled with its high electronegativity, means the introduction of fluorine can effectively lower the energy levels without causing undesired steric hindrance. In addition, fluorination can promote intermolecular and

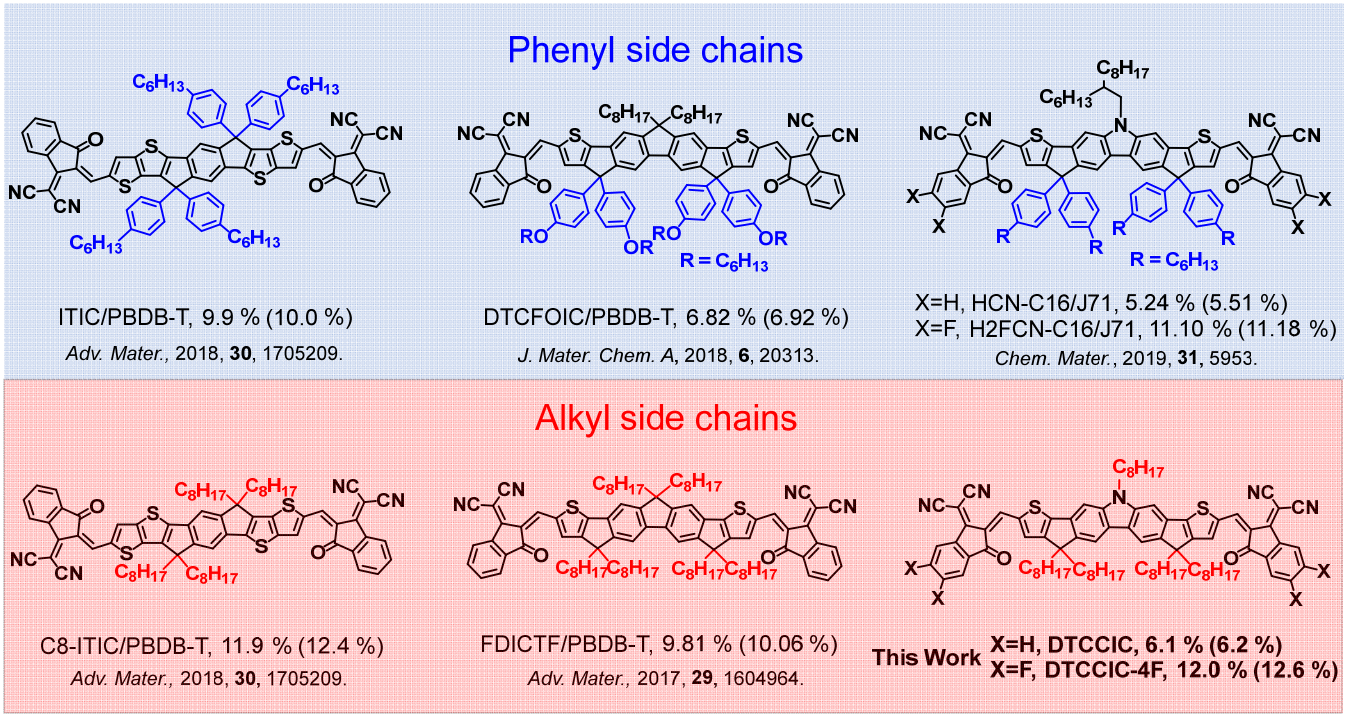

Chart 1. Chemical structures of indacenodithiophene, dithienocyclopentafluorene and dithienocyclopentacarbazole based nonfullerene acceptors with phenyl and alkyl side chains and their average (and best) reported PCE with the specified donor.

intramolecular interactions through noncovalent C–F···S and C–F···H bonds and hence enhance molecular crystallinity and facilitate charge transport.[22-28] Moreover, comparing the 1,1-dicyanomethylene-3-indanone (IC) endgroup with its fluorinated derivative 2-(5,6-difluoro-3-oxo-2,3-dihydro-1H-inden-1-ylidene)malononitrile (IC-4F), the stronger electron-withdrawing effect of the latter can enhance intramolecular charge transfer (ICT) in NFA materials resulted in a red-shift of the absorption spectra of NFAs to the near-IR region, thus enhancing device photocurrent. Several studies have demonstrated that OSCs based on ladder type NFAs with fluorinated endgroups show improved device performance than those based on non-fluorinated counterparts.[29-33]

3,9-Bis(2-methylene-(3-(1,1-dicyanomethylene)-indanone))-5,5,11,11-tetrakis(4-hexylphenyl)-dithieno[2,3-d:2′,3′-d′]-s-indaceno[1,2-b:5,6-b′]dithiophene (ITIC)[34] and 2,2'-[(4,4,9,9-tetrahexyl-4,9-dihydro-s-indaceno[1,2-b:5,6-b']dithiophene-2,7-diyl)bis[methylidyne(3-oxo-1H-indene-2,1(3H)-diylidene)]]bis-propanedinitrile (IDIC)[35] are two of the most representative and widely studied high performance NFAs, where ITIC has phenylalkyl solubilising side chains on the indacenodithieno[3,2-*b*]thiophene core and IDIC has alkyl side chains on the shorter indacenodithiophene core. For the vast majority of NFAs reported so far, arylalkyl chains have been utilized as the solubilizing groups. Partly this is due to synthetic utility, as the aryl groups help to stabilize the carbocation formed during Friedel-Crafts ring closure of the fused core. The use of alkyl chains under similar conditions can sometimes be problematic due to competing side reactions of dehydration or rearrangement. However the arylalkyl group is a relatively bulky solubilizing group and changing to alkyl side chains is expected to strongly influence molecular packing and crystallinity. For example comparison of indacenodithiophene and dithienocyclopentafluorene based NFAs with either octyl (C8-ITIC and FDICTF) or phenyl (ITIC and DTCFOIC) based sidechains shows that the alkyl derivatives have a red shifted and more intense absorption, higher charge carrier mobility, and better overall OSC performance than their counterparts with phenyl side chains (Chart 1 and Table S1).[14,34,36-40]

Based upon the strategy of introducing alkyl sidechain as an effective method to modulate molecular packing and optoelectronics properties, in this work we focused on the development of new acceptors based on a fully alkylated dithienocyclopentacarbazole (DTCC) core end-capped with electron-withdrawing endgroups IC or IC-4F. Such acceptors can be thought of as analogues of the dithienocyclopentafluorene acceptor (FDICTF, Chart 1) in which the central fluorene unit is changed to a more electron rich carbazole unit. Electron rich cores have been shown to enhance the intramolecular charge transfer (ICT) effect and afford a desirable broadening of absorption.[29,41] We further note that changing to a central carbazole unit also results in a reduction in overall alkyl chain density on the acceptor, since the carbazole only has a single octyl sidechain.[42] The resulting acceptors, DTCCIC and DTCCIC-4F show red-shifted absorption spectra with respect to both their fluorine (FDICTF) and phenylalkyl analogues (HCN-C16 and HFCN-C16, Chart 1), with the

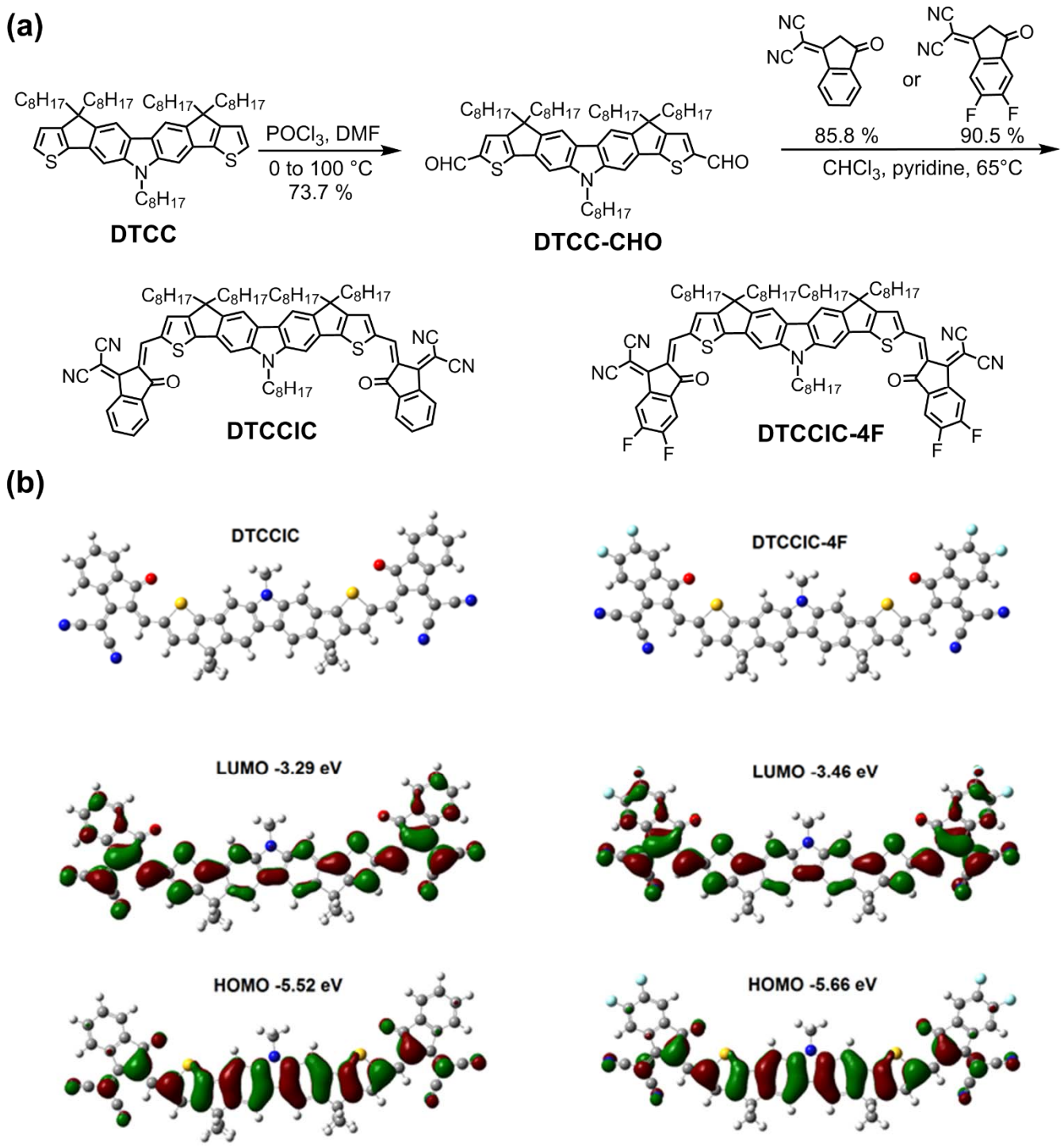

Figure 1. (a) Synthetic route to DTCCIC and DTCCIC-4F. (b) Simulated molecular geometries and LUMO and HOMO distribution of DTCCIC and DTCCIC-4F (alkyls are simplified to methyl) calculated by Gaussian 09 program at B3LYP/6-31G* level.

fluorinated materials exhibiting a narrower band gap and strong molar extinction coefficient than the non-fluorinated version. Notably, we find that OSC devices based on PFBDB-T:DTCCIC-4F achieve an impressive PCE of up to 12.6 % while OSC devices based on PFBDB-T:DTCCIC only obtained a moderate PCE of 6.2 %. The unexpected short circuit current (J_{SC}) and fill factor (FF) losses of PFBDB-T:DTCCIC based devices are ascribed to excessive self-aggregation of DTCCIC and the formation of large phase-separated domains in the active layer, as observed from thermal analysis and microstructure measurements (vide infra).[43,44] Fluorination of the

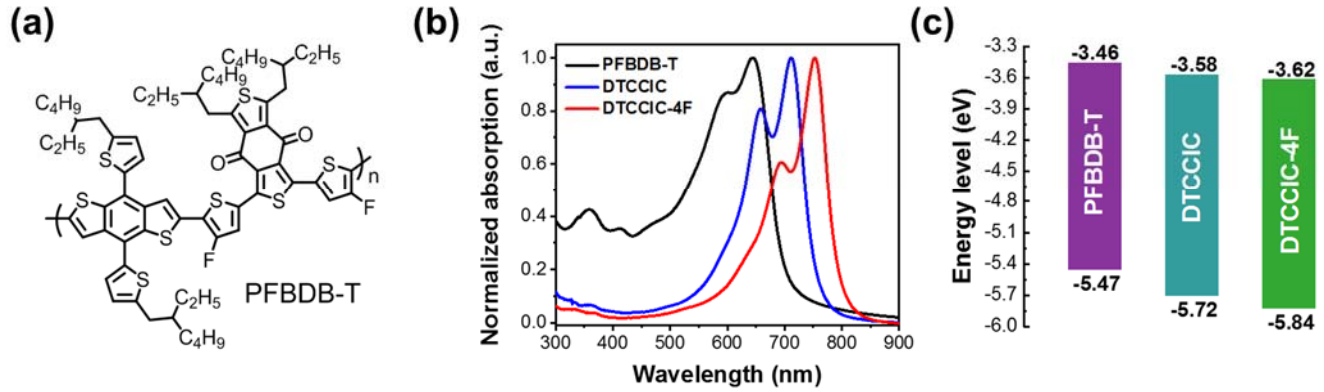

Figure 2. (a) Chemical structure of polymer donor PFBDB-T. (b) Normalized UV-vis absorption spectra of PFBDB-T, DTCCIC and DTCCIC-4F in neat film. (c) Energy levels of PFBDB-T, DTCCIC and DTCCIC-4F.

Table 1. Optical and electrochemical properties of DTCCIC and DTCCIC-4F

		λ_{max}^{abs} (nm)						
Acceptor	T_d (°C)	solution	film	E_g (eV)	ε (mol L^{-1} cm^{-1})	E_{ox}/E_{red} (V)	HOMO (eV)	LUMO (eV)
DTCCIC	317	673	658, 712	1.62	2.02×10^5	1.34/−0.80	−5.72	−3.58
DTCCIC-4F	345	685	695, 753	1.53	2.29×10^5	1.46/−0.76	−5.84	−3.62

endgroups results in a fine tuning of acceptor crystallinity and improved miscibility with the polymer donor PFBDB-T, resulting in a better performance in OSCs.

RESULTS AND DISCUSSION

The synthetic route to DTCCIC and DTCCIC-4F is shown in Figure 1a. More detailed procedures are provided in Scheme S1, Supporting Information. The ladder type fused core DTCC was synthesized according to the literature method.[45] Formylation of the core was achieved by the Vilsmeier-Haack reaction using $POCl_3$ (phosphorus oxychloride) and DMF (dimethylformamide) in good yield. Subsequent Knoevenagel condensation between DTCC-CHO and the electron-withdrawing units IC or IC-4F afforded the target alkylated carbazole acceptors DTCCIC and DTCCIC-4F in high yields. The chemical structure of DTCCIC and DTCCIC-4F were fully characterized by MALDI-TOF MS, ^{1}H and ^{13}C NMR and elemental analysis. Both molecules exhibited good solubility in common organic solvents, such as dichloromethane, chloroform and chlorobenzene at room temperature.

Thermal stability was investigated using thermogravimetric analysis (TGA, Figure S1) under nitrogen atmosphere. The results indicated that DTCCIC and DTCCIC-4F have good thermal stability with a weight loss lower than 5 % up to 317 °C and 345 °C, which meets the requirement of device fabrication. From differential scanning calorimetry (DSC, Figure S2), DTCCIC exhibits an initial broad endotherm at 120 °C on first heating, followed by two sharp endothermic peaks at 225 °C and melting at 272 °C. These latter two transitions were also observed on the second heating/cooling cycle, and on cooling two exothermic peaks were observed. Examination by polarized optical microscopy (POM) suggested that the first endotherm was associated with a crystal-to-crystal phase transition, whilst the second was a melt to an isotropic phase. Fluorination has a significant effect on the thermal behavior with DTCCIC-4F only displaying a distinct thermal transition on the first cycle, with an endothermic peak at 192 °C and no further peaks apparent up to 300 °C. No peaks were observed on cooling, or on subsequent cycles. Examination by POM shows the transition at 192 °C appears to be a crystal-to-crystal transition and that no isotropic phase was observed up to the limit at 280 °C, suggesting the melt is at higher temperature.

Theoretical calculations were conducted using density functional theory (DFT) with the B3LYP/6-31G(d,p) basis set to compare the molecular geometry of DTCCIC and DTCCIC-4F. The two molecules of DTCCIC and DTCC-4F exhibit a similar planar molecular structure, and their frontier molecular orbitals electron distributions are accordant with different electronic property in each building block (Figure 1b). Additionally, the calculations show that DTCCIC-4F has a downshifted highest occupied molecular orbital (HOMO) and lowest unoccupied molecular orbital (LUMO) energy levels, originating from the electron-withdrawing property of the fluorine atoms.

DTCCIC in chloroform solution exhibits strong absorption in the 500 nm to 750 nm region with a maximum extinction coefficient of 2.02×10^5 mol L^{-1} cm^{-1} at 673 nm (Figure S3 and Table 1). As shown in Figure 2b, the film of DTCCIC shows strong absorption in the wavelength region from 500 nm to 800 nm, and the

absorption onset of 765 nm corresponds to an optical bandgap of 1.62 eV. Compared to the HCN-16 acceptor with phenyl sidechains(Chart 1),[40] the maximum absorption peak of DTCCIC in thin film is slightly redshifted by 3 nm to 712 nm with a strong shoulder peak at 658 nm. Fluorination results in a red-shifting of the optical absorption, with the solution and film absorption of DTCCIC-4F at 685 nm and 753 nm respectively. This is consistent with a more intensive intramolecular charge transfer (ICT) effect induced by fluorinated IC-4F endgroups. Moreover, DTCCIC-4F exhibits a higher maximum extinction coefficient (2.29×10^5 mol L^{-1} cm^{-1}) and narrower optical bandgap (1.53 eV) than DTCCIC.

Cyclic voltammetry measurements were employed to investigate the electrochemical properties of DTCCIC and DTCCIC-4F (Figure 2c and Figure S4). The HOMO and LUMO energy levels were calculated from the onset

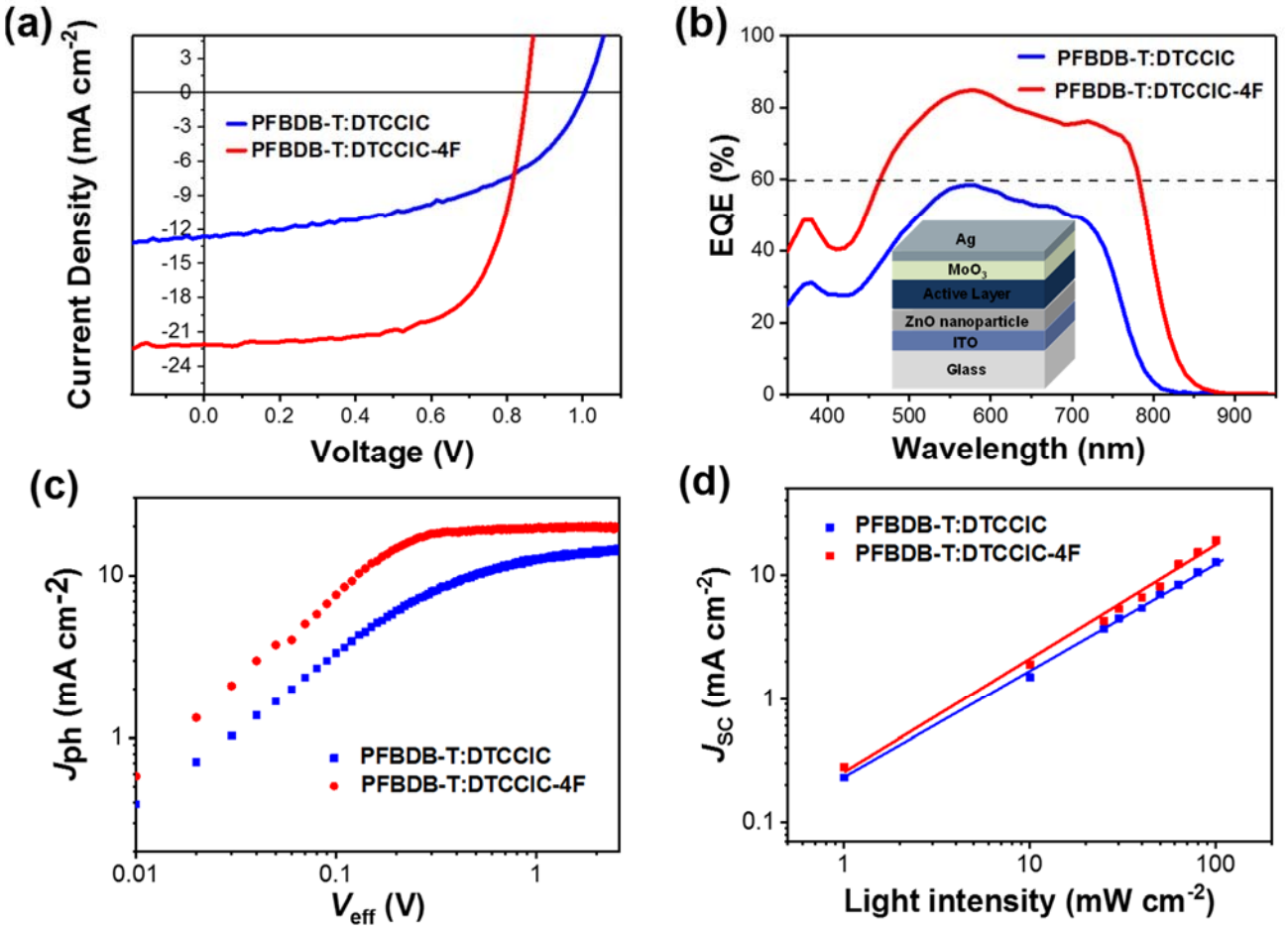

Figure 3. (a) *J*–*V* characteristic curves, (b) EQE spectra, (c) J_{ph} versus V_{eff} characteristics and (d) J_{ph} versus light intensity of the optimized DTCCIC and DTCCIC-4F based OSC devices.

Table 2. Best photovoltaic parameters of OSCs based on PFBDB-T:DTCCIC and PFBDB-T:DTCCIC-4F as the active layer. The average values and standard deviation data of 20 devices are in the brackets. RT indicates room temperature or not annealed.

Active layer	Annealing	V_{OC} (V)	J_{SC} (mA cm^{-2})	FF	PCE (%)
PFBDB-T:DTCCIC	RT	1.01 (1.0 ± 0.01)	12.6 (12.3 ± 0.3)	0.48 (0.47 ± 0.01)	6.2 (5.8 ± 0.4)
PFBDB-T:DTCCIC	100 °C	1.01 (1.0 ± 0.01)	12.0 (11.7 ± 0.2)	0.44 (0.43 ± 0.01)	5.3 (5.0 ± 0.3)
PFBDB-T:DTCCIC-4F	RT	0.84 (0.82 ± 0.02)	21.9 (21.7 ± 0.2)	0.63 (0.62 ± 0.01)	11.6 (11.0 ± 0.6)
PFBDB-T:DTCCIC-4F	100 °C	0.85 (0.84 ± 0.01)	22.1 (21.9 ± 0.3)	0.67 (0.66 ± 0.01)	12.6 (12.1 ± 0.5)

oxidation and reduction potentials and calibrated by ferrocene/ferrocenium (F_C/F_C^+, –4.8 eV below vacuum). The HOMO energy levels of DTCCIC and DTCCIC-4F are estimated to be –5.72 eV and –5.84 eV and the LUMO energy levels are –3.58 eV and –3.62 eV, respectively. The slightly downshifted energy levels of DTCCIC-4F are

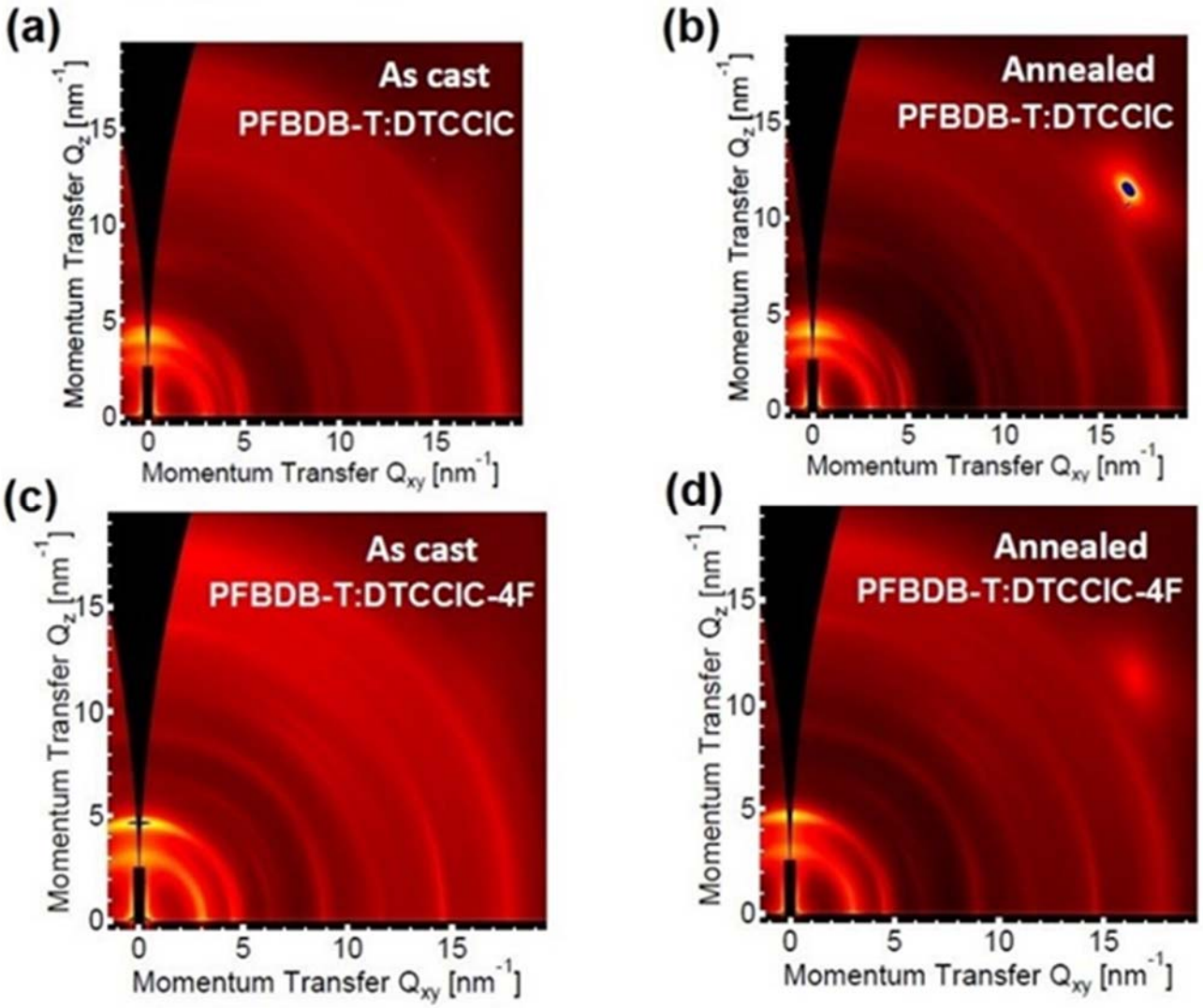

Figure 4. 2D GIWAXS patterns for PFBDB-T:DTCCIC (a, b) and PFBDB-T:DTCCIC-4F (c, d) blend films. Results for as-cast (a, c) and annealed (b, d) films are shown.

related to the electron-withdrawing property of fluorine, which is also in agreement with theoretical DFT calculation.

Inverted OSC devices were utilized to investigate the performance of DTCCIC and DTCCIC-4F as non-fullerene acceptors using an ITO/ZnO nanoparticle/active layer/MoO_3/Ag structure. The previously reported PFBDB-T[14] was utililzed as the donor polymer due to its well matched energy levels and non-overlapping absorption spectra (Figure 2). Devices were optimized used various blend ratios and annealing treatments (see supporting information). The current density–voltage (*J*–*V*) curves of the optimal devices based on DTCCIC and DTCCIC-4F are shown as Figure 3a, and their corresponding photovoltaic parameters are summarized in Table 2. PFBDB-T:DTCCIC-based devices showed 6.2 % PCE with a high V_{OC} of 1.01V, benefitting from the high-lying LUMO energy level of DTCCIC. Encouragingly, compared with PFBDB-T:DTCCIC-based devices, PFBDB-T:DTCCIC-4F-based devices achieved a much higher J_{SC} of 21.9 mA cm^{-2}, better fill factor of 0.63, and improved PCE of 11.6 %, due to their broader and stronger complementary absorption, albeit with a lower V_{OC} of 0.84 V. After thermal annealing of the active layer, PFBDB-T:DTCCIC-4F based devices exhibited better performance than the unannealed devices while the performance of PFBDB-T:DTCCIC based devices slightly decreased. The morphology of neat DTCCIC and DTCCIC-4F films and their blends with PFBDB-T were further studied to explain these phenomenon. Interestingly, in both cases annealing affected only the fill factor, with the V_{OC} and J_{SC} both remaining unchanged.

External quantum efficiency (EQE) measurements were performed to determine the spectral origin of the photocurrent and verify the J_{SC} values for optimal DTCCIC

and DTCCIC-4F based devices. As shown in Figure 3b, the DTCCIC-4F based devices reach a maximum EQE value of 84 % and retain an average of over 60 % across the range of 460 nm to 780 nm, a higher photo-to-current response than that of DTCCIC based devices across the whole visible range, indicating a more efficient photoelectron conversion process. Additionally, DTCCIC-4F based devices displayed a redshifted photocurrent response edge compared to the DTCCIC based device, in accordance with the trend of their corresponding films absorption profiles. The broader and increased EQE values of the DTCCIC-4F based device is in good agreement with the observed higher J_{SC} and demonstrates the beneficial effect of fluorination of DTCCIC on the photo-harvesting ability of these devices. The J_{SC} values calculated from the EQE curves are (11.92 and 20.89) mA cm^{-2} for the DTCCIC and DTCCIC-4F based devices, respectively, which are close to those from the *J–V* measurements.

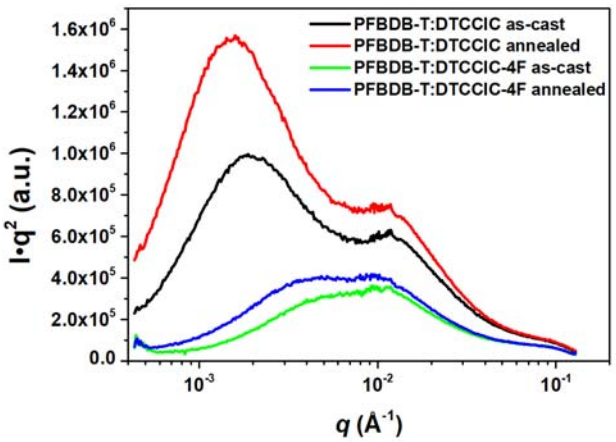

Figure 5. R-SoXS scattering profiles of as-cast and annealed films of PFBDB-T:DTCCIC and PFBDB-T:DTCCIC-4F. An energy of 283.9 eV was used for the PFBDB-T:DTCCIC blend while an energy of 283.6 eV was used for the PFBDB-T:DTCCIC-4F. In both cases the photon energy chosen was found to maximize scattering contrast. Note that q² scaling is used to magnify the differences in scatter. Profiles represent spatial material fluctuations within the film. Unscaled data is provided in the supporting information.

The exciton dissociation and charge recombination behavior was investigated in the optimized devices for each blend, using a combination of photocurrent (J_{ph}) versus the effective applied voltage (V_{eff}) and light-intensity measurements of J_{SC}.[46] The devices exhibited significantly different behaviour in their trends of J_{ph} versus V_{eff} (Figure 3c), with J_{ph} for DTCCIC devices not saturating (J_{sat}) until V_{eff} exceeds 2.3 V, whereas DTCCIC-4F saturated at much lower values. The ratio of J_{ph}/J_{sat} allows the charge dissociation and collection probabilities of the blends to be estimated, with the DTCCIC-4F being much higher than than the DTCCIC based device under both short circuit condition (97.8 % for DTCCIC-4F vs 89.4 % for DTCCIC) and maximal power output conditions (90.8 % for DTCCIC-4F vs 59.9 % for DTCCIC). The dependence of the J_{SC} on the light-intensity is shown in Figure 3d for both blends. A steeper slope (0.913) is found for for the DTCCIC-4F based device compared to the DTCCIC based device (0.878), suggesting lower bimolecular recombination in the DTCCIC-4F based device, in agreement with its higher extraction probability.

The electron and hole mobilities of PFBDB-T:DTCCIC and PFBDB-T:DTCCIC-4F blends were measured using the space-charge-limited current (SCLC) method. Device structures comprising ITO/ZnO nanoparticle/active layer/Ca/Al were utilized for electrons and ITO/PEDOT:PSS/active layer/MoO_3/Ag for holes.. As shown in Figure S5 and Table S2, the electron and hole mobilities for PFBDB-T:DTCCIC blends were measured to be (2.15×10^{-6} and 4.9×10^{-5}) cm^{-2} V^{-1} s^{-1}, respectively. On the contrary, PFBDB-T:DTCCIC-4F blend films exhibited electron and hole mobilities of (4.27×10^{-6} and 9.26×10^{-5}) cm^{-2} V^{-1} s^{-1}, which are higher than those of PFBDB-T:DTCCIC blend films. This improved charge transport also helps to explain the higher observed current for DTCCIC-4F based devices.

Grazing-incidence wide-angle X-ray scattering (GIWAXS) was applied to investigate the microstructural differences between neat DTCCIC and DTCCIC-4F and their blends. Figure S6 shows the GIWAXS results of as-cast and annealed neat films. Both DTCCIC and DTCCIC-4F exhibit complex scattering patterns consistent with highly crystalline materials. Neat DTCCIC films exhibit a higher degree of mosaicity (spreading of crystal plane orientations) with neat DTCCIC-4F films being more strongly oriented. In both cases, annealing of neat films leads to an improvement in the degree of crystallinity. The 2D GIWAXS patterns of the blends are shown in Figure 4. Scattering from the acceptor phases in both blends is characterized by powder-like diffraction rings indicating a significantly higher degree of mosaicity. The scattering features from the acceptor molecules are also less sharp, indicating reduced crystallinity in the blend, although these molecules still exhibit a higher degree of crystallinity in the bulk heterojunction blend compared to other acceptors such as ITIC and ITIC-C8.[14] Scattering from the polymer can also be discerned, characterized by a broad lamellar stacking peak at ≈ 3 nm^{-1} and broad π-π stacking peak at ≈ 17 nm^{-1}.[14] The effect of annealing on the GIWAXS patterns is slight, with the PFBDB-T:DTCCIC blend showing some sharpening of the diffraction features (see 1D line profiles in the Supporting Information), while the GIWAXS patterns of the PFBDB-T:DTCCIC-4F not showing any obvious change.

Resonant soft X-ray scattering (R-SoXS) was performed to probe the nanoscale to mesoscale morphology, see Figure 5. The scattering profile of the PFBDB-T:DTCCIC blend is characterized by a scattering feature at ≈ 1.5×10^{-3} Å^{-1} and ≈ 10^{-2} Å^{-1}. The scattering feature at ≈ 1.5×10^{-3} Å^{-1} would correspond to a spatial fluctuation at ≈ 400 nm which is much larger than the optimum domain spacing for an efficient bulk heterojunction solar cell. In contrast the PFBDB-T:DTCCIC-4F blend only shows scattering at

higher q values corresponding to a finer morphology. In particular the prominent scattering feature at ≈ 1.5×10^{-3} Å^{-1} observed in the PFBDB-T:DTCCIC blend is missing for the PFBDB-T:DTCCIC-4F blend, with a broad scattering profile instead seen extending between ≈ 3×10^{-3} Å^{-1} to ≈ 2×10^{-2} Å^{-1} corresponding to spatial fluctuations ranging from ≈ 30 nm to ≈ 200 nm. This large difference in the characteristic spatial fluctuations for PFBDB-T:DTCCIC and PFBDB-T:DTCCIC-4F can help explain the large difference in solar cell efficiency between the two blends, with the morphology of the PFBDB-T:DTCCIC blend being too coarse for efficient photovoltaic operation. For both blends annealing leads to an increase in scattering intensity and a slight shift in the scattering profiles to the left, corresponding to a coarsening of the blends and increase in domain purity. For the case of the PFBDB-T:DTCCIC blend this coarsening leads to a worsening of device performance since the domains are likely already too large. For the case of the PFBDB-T:DTCCIC-4F blend this slight coarsening and increase in domain purity seems to benefit solar cell performance.

The morphologies of the PFBDB-T:DTCCIC and PFBDB-T:DTCCIC-4F blend layers were also studied by tapping-mode atomic force microscopy (AFM). As observed from the AFM images (Figure S8), the neat DTCCIC and DTCCIC-4F films shows large crystallites consistent with the GIWAXS results that found these materials to be highly crystalline. The surface morphologies of the blends also show features consistent with acceptor aggregates, with the PFBDB-T:DTCCIC blend showing larger feature sizes than the PFBDB-T:DTCCIC-4F blend consistent with the R-SoXS results, indicating that the spatial fluctuations observed likely correspond to domain features.

CONCLUSIONS

In conclusion, we designed and synthesized two new ladder type non-fullerene acceptors DTCCIC and DTCCIC-4F based on alkylated ladder dithienocyclopentacarbazole core endcapped with non-fluorinated or fluorinated electron-withdrawing units (IC or IC-4F), and investigated the alkylation and fluorination effects on the morphological, optical, electronic and photovoltaic device properties. By replacing phenyl side chains, fully alkylated DTCCIC and DTCCIC-4F exhibit strong molecular aggregation and stronger redshifted absorption. Compared to non-fluorinated DTCCIC, fluorinated DTCCIC-4F exhibits further redshifted absorption spectra with a smaller optical bandgap of 1.53 eV and downshifted energy levels. PFBDB-T:DTCCIC-4F blend shows better nanoscale morphology and increased domain purity relative to PFBDB-T:DTCCIC blend. OSC devices based on PFBDB-T:DTCCIC-4F blends exhibit PCEs of 12.6 %, significantly higher than those of PFBDB-T:DTCCIC based devices (6.2 %) and among the highest efficiencies for dithienocyclopentacarbazole based non-fullerene acceptors. These results further highlight that end group fluorination is an important approach to enhance overall photovoltaic performance compared to the analogous non-fluorinated material.

ASSOCIATED CONTENT

Supporting Information

Experimental procedures including synthesis, device fabrication and additional characterization data, such as NMR, TGA, DSC, UV–vis absorption, CV data, SCLC, AFM, GIWAXS, R-SoXS. This material is available free of charge via the Internet at http://pubs.acs.org.

AUTHOR INFORMATION

Corresponding Author

* E-mail: m.heeney@imperial.ac.uk.

Notes

The authors declare no competing financial interest.

ACKNOWLEDGMENT

Imperial College authors thank the China Scholarship Council (CSC) via the CSC Imperial Scholarship, the Daphne Jackson Trust (supported by RSC and EPSRC), the Global Research Laboratory Program of the National Research Foundation (NRF) funded by the Ministry of Science, ICT & Future Planning (NRF-2017K1A1A2013153), and the Royal Society and Wolfson Foundation (for Royal Society Wolfson Fellowship) for funding. ZF thanks 'the National Science Foundation of China (NSFC, Project No. 21975176). TA acknowledges the King Abdullah University of Science and Technology (KAUST) for financial support. QH acknowledges valuable discussions with Dr Cenqi Yan. This work was performed in part on the SAXS/WAXS beamline[47] at the Australian Synchrotron, part of ANSTO. This research used the Spectroscopy Soft and Tender (SST-1) beamline of the National Synchrotron Light Source II, a U.S. Department of Energy (DOE) Office of Science User Facility operated for the DOE Office of Science by Brookhaven National Laboratory under Contract No. DE-SC0012704. CRM acknowledges travel funding provided by the International Synchrotron Access Program (ISAP) managed by the Australian Synchrotron, part of ANSTO (AS/IA192/15608), and funded by the Australian Government

REFERENCES

(1) Yuan, J.; Zhang, Y.; Zhou, L.; Zhang, G.; Yip, H.-L.; Lau, T.-K.; Lu, X.; Zhu, C.; Peng, H.; Johnson, P. A.; Leclerc, M.; Cao, Y.; Ulanski, J.; Li, Y.; Zou, Y. Single-Junction Organic Solar Cell with over 15 % Efficiency Using Fused-Ring Acceptor with Electron-Deficient Core. *Joule* **2019**, *3*, 1140-1151.

(2) Cui, Y.; Yao, H.; Zhang, J.; Zhang, T.; Wang, Y.; Hong, L.; Xian, K.; Xu, B.; Zhang, S.; Peng, J.; Wei, Z.; Gao, F.; Hou, J. Over 16 % Efficiency Organic Photovoltaic Cells Enabled by a Chlorinated Acceptor with Increased Open-Circuit Voltages. *Nat. Commun.* **2019**, *10*, 2515.

(3) Fan, B.; Zhang, D.; Li, M.; Zhong, W.; Zeng, Z.; Ying, L.; Huang, F.; Cao, Y. Achieving over 16 % Efficiency for Single-Junction Organic Solar Cells. *Sci. China Chem.* **2019**, *62*, 746-752.

(4) Zhang, G.; Zhao, J.; Chow, P. C. Y.; Jiang, K.; Zhang, J.; Zhu, Z.; Zhang, J.; Huang, F.; Yan, H. Nonfullerene Acceptor Molecules for Bulk Heterojunction Organic Solar Cells. *Chem. Rev.* **2018**, *118*, 3447-3507.

(5) Nielsen, C. B.; Holliday, S.; Chen, H.-Y.; Cryer, S. J.; McCulloch, I. Non-Fullerene Electron Acceptors for Use in Organic Solar Cells. *Acc. Chem. Res.* **2015**, *48*, 2803-2812.
(6) Cheng, P.; Li, G.; Zhan, X.; Yang, Y. Next-Generation Organic Photovoltaics Based on Non-Fullerene Acceptors. *Nat. Photon.* **2018**, *12*, 131-142.
(7) Yan, C.; Barlow, S.; Wang, Z.; Yan, H.; Jen, A. K. Y.; Marder, S. R.; Zhan, X. Non-Fullerene Acceptors for Organic Solar Cells. *Nat. Rev. Mater.* **2018**, *3*, 18003.
(8) Wadsworth, A.; Moser, M.; Marks, A.; Little, M. S.; Gasparini, N.; Brabec, C. J.; Baran, D.; McCulloch, I. Critical Review of the Molecular Design Progress in Non-Fullerene Electron Acceptors Towards Commercially Viable Organic Solar Cells. *Chem. Soc. Rev.* **2018**, *48*, 1596-1625.
(9) Hou, J.; Inganas, O.; Friend, R. H.; Gao, F. Organic Solar Cells Based on Non-Fullerene Acceptors. *Nat. Mater.* **2018**, *17*, 119-128.
(10) Jiang, Z.-Q.; Wang, T.-T.; Wu, F.-P.; Lin, J.-D.; Liao, L.-S. Recent Advances in Electron Acceptors with Ladder-Type Backbone for Organic Solar Cells. *J. Mater. Chem. A* **2018**, *6*, 17256-17287.
(11) Wu, J. S.; Cheng, S. W.; Cheng, Y. J.; Hsu, C. S. Donor-Acceptor Conjugated Polymers Based on Multifused Ladder-Type Arenes for Organic Solar Cells. *Chem. Soc. Rev.* **2015**, *44*, 1113-1154.
(12) Lin, Y.; Zhan, X. Designing Efficient Non-Fullerene Acceptors by Tailoring Extended Fused-Rings with Electron-Deficient Groups. *Adv. Energy Mater.* **2015**, *5*, 1501063.
(13) Liu, W.; Zhang, J.; Zhou, Z.; Zhang, D.; Zhang, Y.; Xu, S.; Zhu, X. Design of a New Fused-Ring Electron Acceptor with Excellent Compatibility to Wide-Bandgap Polymer Donors for High-Performance Organic Photovoltaics. *Adv. Mater.* **2018**, *30*, 1800403.
(14) Fei, Z.; Eisner, F. D.; Jiao, X.; Azzouzi, M.; Röhr, J. A.; Han, Y.; Shahid, M.; Chesman, A. S. R.; Easton, C. D.; McNeill, C. R.; Anthopoulos, T. D.; Nelson, J.; Heeney, M. An Alkylated Indacenodithieno[3,2-b]thiophene-Based Nonfullerene Acceptor with High Crystallinity Exhibiting Single Junction Solar Cell Efficiencies Greater than 13 % with Low Voltage Losses. *Adv. Mater.* **2018**, *30*, 1705209.
(15) Aldrich, T. J.; Matta, M.; Zhu, W.; Swick, S. M.; Stern, C. L.; Schatz, G. C.; Facchetti, A.; Melkonyan, F. S.; Marks, T. J. Fluorination Effects on Indacenodithienothiophene Acceptor Packing and Electronic Structure, End-Group Redistribution, and Solar Cell Photovoltaic Response. *J. Am. Chem. Soc.* **2019**, *141*, 3274-3287.
(16) Chen, F. X.; Xu, J. Q.; Liu, Z. X.; Chen, M.; Xia, R.; Yang, Y.; Lau, T. K.; Zhang, Y.; Lu, X.; Yip, H. L.; Jen, A. K.; Chen, H.; Li, C. Z. Near-Infrared Electron Acceptors with Fluorinated Regioisomeric Backbone for Highly Efficient Polymer Solar Cells. *Adv. Mater.* **2018**, *30*, 1705416.
(17) Zhang, Q.; Kelly, M. A.; Bauer, N.; You, W. The Curious Case of Fluorination of Conjugated Polymers for Solar Cells. *Acc. Chem. Res.* **2017**, *50*, 2401-2409.
(18) Zhao, W.; Li, S.; Yao, H.; Zhang, S.; Zhang, Y.; Yang, B.; Hou, J. Molecular Optimization Enables over 13 % Efficiency in Organic Solar Cells. *J. Am. Chem. Soc.* **2017**, *139*, 7148-7151.
(19) Tang, M. L.; Bao, Z. Halogenated Materials as Organic Semiconductors. *Chem. Mater.* **2011**, *23*, 446-455.
(20) Kawashima, K.; Fukuhara, T.; Suda, Y.; Suzuki, Y.; Koganezawa, T.; Yoshida, H.; Ohkita, H.; Osaka, I.; Takimiya, K. Implication of Fluorine Atom on Electronic Properties, Ordering Structures, and Photovoltaic Performance in Naphthobisthiadiazole-Based Semiconducting Polymers. *J. Am. Chem. Soc.* **2016**, *138*, 10265-10275.
(21) Reichenbächer, K.; Süss, H. I.; Hulliger, J. Fluorine in Crystal Engineering—"the Little Atom That Could". *Chem. Soc. Rev.* **2005**, *34*, 22-30.
(22) Boufflet, P.; Han, Y.; Fei, Z.; Treat, N. D.; Li, R.; Smilgies, D.-M.; Stingelin, N.; Anthopoulos, T. D.; Heeney, M. Using Molecular Design to Increase Hole Transport: Backbone Fluorination in the Benchmark Material Poly(2,5-bis(3-alkylthiophen-2-yl)thieno[3,2-b]-thiophene (pBTTT). *Adv. Funct. Mater.* **2015**, *25*, 7038-7048.
(23) Fei, Z.; Boufflet, P.; Wood, S.; Wade, J.; Moriarty, J.; Gann, E.; Ratcliff, E. L.; McNeill, C. R.; Sirringhaus, H.; Kim, J.-S.; Heeney, M. Influence of Backbone Fluorination in Regioregular Poly(3-alkyl-4-fluoro)thiophenes. *J. Am. Chem. Soc.* **2015**, *137*, 6866-6879.
(24) Liu, J.; Ma, L. K.; Lin, H.; Zhang, L.; Li, Z.; Law, W. K.; Shang, A.; Hu, H.; Ma, W.; Yan, H. A Donor Polymer Based on a Difluorinated Pentathiophene Unit Enabling Enhanced Performance for Nonfullerene Organic Solar Cells. *Small Methods* **2018**, *2*, 1700415.
(25) Dai, S.; Zhao, F.; Zhang, Q.; Lau, T. K.; Li, T.; Liu, K.; Ling, Q.; Wang, C.; Lu, X.; You, W.; Zhan, X. Fused Nonacyclic Electron Acceptors for Efficient Polymer Solar Cells. *J. Am. Chem. Soc.* **2017**, *139*, 1336-1343.
(26) Yang, Y.; Wang, K.; Li, G.; Ran, X.; Song, X.; Gasparini, N.; Zhang, Q.-Q.; Lai, X.; Guo, X.; Meng, F.; Du, M.; Huang, W.; Baran, D. Fluorination Triggered New Small Molecule Donor Materials for Efficient As-Cast Organic Solar Cells. *Small* **2018**, *14*, 1801542.
(27) Kharandiuk, T.; Hussien, E. J.; Cameron, J.; Petrina, R.; Findlay, N. J.; Naumov, R.; Klooster, W. T.; Coles, S. J.; Ai, Q.; Goodlett, S.; Risko, C.; Skabara, P. J. Noncovalent Close Contacts in Fluorinated Thiophene–Phenylene–Thiophene Conjugated Units: Understanding the Nature and Dominance of O···H versus S···F and O···F Interactions with Respect to the Control of Polymer Conformation. *Chem. Mater.* **2019**, *31*, 7070-7079.
(28) Zhang, A.; Xiao, C.; Wu, Y.; Li, C.; Ji, Y.; Li, L.; Hu, W.; Wang, Z.; Ma, W.; Li, W. Effect of Fluorination on Molecular Orientation of Conjugated Polymers in High Performance Field-Effect Transistors. *Macromolecules* **2016**, *49*, 6431-6438.
(29) Sun, J.; Ma, X.; Zhang, Z.; Yu, J.; Zhou, J.; Yin, X.; Yang, L.; Geng, R.; Zhu, R.; Zhang, F.; Tang, W. Dithieno[3,2-b:2′,3′-d]pyrrol Fused Nonfullerene Acceptors Enabling Over 13 % Efficiency for Organic Solar Cells. *Adv. Mater.* **2017**, *30*, 1707150.
(30) Lv, R.; Chen, D.; Liao, X.; Chen, L.; Chen, Y. A Terminally Tetrafluorinated Nonfullerene Acceptor for Well-Performing Alloy Ternary Solar Cells. *Adv. Funct. Mater.* **2019**, *29*, 1805872.
(31) Pan, F.; Zhang, L.; Jiang, H.; Yuan, D.; Nian, Y.; Cao, Y.; Chen, J. As-Cast Ternary Polymer Solar Cells Based on a Nonfullerene Acceptor and Its Fluorinated Counterpart Showing Improved Efficiency and Good Thickness Tolerance. *J. Mater. Chem. A* **2019**, *7*, 9798-9806.
(32) Zhao, F.; Dai, S.; Wu, Y.; Zhang, Q.; Wang, J.; Jiang, L.; Ling, Q.; Wei, Z.; Ma, W.; You, W.; Wang, C.; Zhan, X. Single-Junction Binary-Blend Nonfullerene Polymer Solar Cells with 12.1 % Efficiency. *Adv. Mater.* **2017**, *29*, 1700144.
(33) Kan, B.; Zhang, J.; Liu, F.; Wan, X.; Li, C.; Ke, X.; Wang, Y.; Feng, H.; Zhang, Y.; Long, G.; Friend, R. H.; Bakulin, A. A.; Chen, Y. Fine-Tuning the Energy Levels of a Nonfullerene Small-Molecule Acceptor to Achieve a High Short-Circuit Current and a Power Conversion Efficiency over 12 % in Organic Solar Cells. *Adv. Mater.* **2017**, *30*, 1704904.
(34) Lin, Y.; Wang, J.; Zhang, Z.-G.; Bai, H.; Li, Y.; Zhu, D.; Zhan, X. An Electron Acceptor Challenging Fullerenes for Efficient Polymer Solar Cells. *Adv. Mater.* **2015**, *27*, 1170-1174.
(35) Lin, Y.; He, Q.; Zhao, F.; Huo, L.; Mai, J.; Lu, X.; Su, C.-J.; Li, T.; Wang, J.; Zhu, J.; Sun, Y.; Wang, C.; Zhan, X. A Facile Planar Fused-Ring Electron Acceptor for As-Cast Polymer Solar

Cells with 8.71 % Efficiency. *J. Am. Chem. Soc.* **2016**, *138*, 2973-2976.

(36) Guo, W.; Zhao, B.; Xin, J.; Liu, H.; Mi, Y.; Zhang, J.; Guo, Z.; Wei, W.; Ma, W.; Gao, C.; An, Z. Non-Fullerene Small Molecular Acceptors Based on Dithienocyclopentafluorene and Dithienocyclopentacarbazole Cores for Polymer Solar Cells. *Dyes and Pigments* **2017**, *144*, 48-57.

(37) Qiu, N.; Zhang, H.; Wan, X.; Li, C.; Ke, X.; Feng, H.; Kan, B.; Zhang, H.; Zhang, Q.; Lu, Y.; Chen, Y. A New Nonfullerene Electron Acceptor with a Ladder Type Backbone for High-Performance Organic Solar Cells. *Adv. Mater.* **2017**, *29*, 1604964.

(38) Cao, Q.; Xiong, W.; Chen, H.; Cai, G.; Wang, G.; Zheng, L.; Sun, Y. Design, Synthesis, and Structural Characterization of the First Dithienocyclopentacarbazole-Based N-Type Organic Semiconductor and Its Application in Non-Fullerene Polymer Solar Cells. *J. Mater. Chem. A* **2017**, *5*, 7451-7461.

(39) Yin, P.; Zheng, T.; Wu, Y.; Liu, G.; Zhang, Z.-G.; Cui, C.; Li, Y.; Shen, P. Achieving Efficient Thick Active Layer and Large Area Ternary Polymer Solar Cells by Incorporating a New Fused Heptacyclic Non-Fullerene Acceptor. *J. Mater. Chem. A* **2018**, *6*, 20313-20326.

(40) Tu, Q.; Ma, Y.; Zhou, X.; Ma, W.; Zheng, Q. Enhancing the Photovoltaic Performance of Ladder-Type Dithienocyclopentacarbazole-Based Nonfullerene Acceptors through Fluorination and Side-Chain Engineering. *Chem. Mater.* **2019**, *31*, 5953-5963.

(41) Huang, C.; Liao, X.; Gao, K.; Zuo, L.; Lin, F.; Shi, X.; Li, C.-Z.; Liu, H.; Li, X.; Liu, F.; Chen, Y.; Chen, H.; Jen, A. K. Y. Highly Efficient Organic Solar Cells Based on S,N-Heteroacene Non-Fullerene Acceptors. *Chem. Mater.* **2018**, *30*, 5429-5434.

(42) Al-Naamani, E.; Gopal, A.; Ide, M.; Osaka, I.; Saeki, A. Exploring Alkyl Chains in Benzobisthiazole-Naphthobisthiadiazole Polymers: Impact on Solar-Cell Performance, Crystalline Structures, and Optoelectronics. *ACS Appl. Mater. Interfaces* **2017**, *9*, 37702-37711.

(43) Li, Y.; Zheng, N.; Yu, L.; Wen, S.; Gao, C.; Sun, M.; Yang, R. A Simple Phenyl Group Introduced at the Tail of Alkyl Side Chains of Small Molecular Acceptors: New Strategy to Balance the Crystallinity of Acceptors and Miscibility of Bulk Heterojunction Enabling Highly Efficient Organic Solar Cells. *Adv. Mater.* **2019**, *31*, 1807832.

(44) Yan, C.; Yang, T.; Gao, W.; Xiao, Y.; Li, Y.; Lu, X.; Yang, C.; Li, G. Chlorination Strategy-Induced Abnormal Nanomorphology Tuning in High-Efficiency Organic Solar Cells: A Study of Phenyl-Substituted Benzodithiophene-Based Nonfullerene Acceptors. *Solar RRL* **2019**, *3*, 1900262.

(45) Lee, T.-H.; Wu, K.-Y.; Lin, T.-Y.; Wu, J.-S.; Wang, C.-L.; Hsu, C.-S. Role of the Comonomeric Units in Reaching Linear Backbone, High Solid-State Order and Charge Mobilities in Heptacyclic Arene-Based Alternating Copolymers. *Macromolecules* **2013**, *46*, 7687-7695.

(46) Proctor, C. M.; Kuik, M.; Nguyen, T.-Q. Charge Carrier Recombination in Organic Solar Cells. *Prog. Polym. Sci.* **2013**, *38*, 1941-1960.

(47) Kirby, N. M.; Mudie, S. T.; Hawley, A. M.; Cookson, D. J.; Mertens, H. D. T.; Cowieson, N.; Samardzic-Boban, V. A Low-Background-Intensity Focusing Small-Angle X-Ray Scattering Undulator Beamline. *J. Appl. Crystallogr.* **2013**, *46*, 1670-1680.

Insert Table of Contents artwork here